

# Spin-Orbit Coupling Induced Degeneracy in the Anisotropic Unconventional Superconductor $\text{UTe}_2$

Alexander B. Shick

*Institute of Physics, Czech Academy of Science, Na Slovance 2, CZ-18221 Prague, Czech Republic*

Warren E. Pickett\*

*University of California Davis, Davis CA 95616\**

(Dated: August 6, 2019)

The orthorhombic uranium dichalcogenide  $\text{UTe}_2$  displays superconductivity below 1.7 K, with the anomalous feature of retaining 50% of normal state (ungapped) carriers, according to heat capacity data from two groups. Incoherent transport that crosses over from above 50 K toward a low temperature, Kondo lattice Fermi liquid regime indicates strong magnetic fluctuations and the need to include correlation effects in theoretical modeling. We report density functional theory plus Hubbard U (DFT+U) results for  $\text{UTe}_2$  to provide a platform for modeling its unusual behavior, focusing on ferromagnetic (FM, time reversal breaking) long range correlations along the  $\hat{a}$  axis as established by magnetization measurements and confirmed by our calculations. States near the Fermi level are dominated by the  $j = \frac{5}{2}$  configuration, with the  $j_z = \pm \frac{1}{2}$  sectors being effectively degenerate and half-filled. Unlike the small-gap insulating nonmagnetic electronic spectrum, the FM Fermi surfaces are large (strongly metallic) and display low dimensional features, reminiscent of the FM superconductor  $\text{UGe}_2$ .

PACS numbers:

## I. INTRODUCTION

Crystal symmetries have played a crucial role in classification of superconducting gaps, with the well studied options being nodeless, point node, or line node gaps. These classes have different types of low energy excitations, as observed in spectroscopic, thermodynamic, and transport properties. Symmetries also play a central role in the topological classification of normal crystalline materials, leading to topological versus ‘trivial’ insulators, Weyl semimetals, and multi-Weyl semimetals, as well as some more esoteric classes. A conjunction of these criteria was discovered by Agterberg, Brydon, and Timm (ABT)[1], who established the possibility of a superconducting phase with topological protection that retains an *area* of gapless excitations, called by them a Bogoliubov Fermi surface (BFS). The BFS phase combines a conventionally gapped region of Fermi surface (FS) with an ungapped portion – a normal electronic Fermi surface – resulting in a new phase of matter which for now is called the BFS phase.

This theoretical development is especially prescient because of recent indications of superconducting phases in which a finite fraction of carriers remain ungapped at temperature  $T=0$ . A definitive indication is a non-zero Sommerfeld specific heat coefficient well below the superconducting critical temperature  $T_c$ , when the sample is sufficiently free of second phases. One example is the Fe(S,Se) alloy system,[2, 3] and other possible examples have been mentioned by ABT.[1] The basic need at this

time is to obtain a realistic band structure including the requisite aspects that will form the platform for inclusion of additional (viz. dynamic) effects. We focus on the newly synthesized actinide chalcogenide  $\text{UTe}_2$ .

$\text{UTe}_2$ , which crystallizes in an orthorhombic  $Immm$  structure[4] (space group #71) shown in Fig. 1, has been suggested by Ran and collaborators[5] to provide a new phase of superconducting matter below  $T_c=1.7\text{K}$  in which half of the electrons become superconducting and half remain normal (thus with Fermi surfaces), based on heat capacity data. The implication is that, at  $T_c$ , some additional symmetry is broken beyond the usual broken gauge symmetry. While no magnetic ordering is detected, it was proposed that half of the fermionic excitations (spin up, for want of a better characterization) become superconducting while the spin down fermions remain in the normal conducting state. Confirmation of the basic properties has been provided by Aoki *et al.* [6], who extended some of the measurements. That this behavior occurs in a U-based compound brings to mind the three U-based ferromagnetic superconductors  $\text{UGe}_2$ ,  $\text{URhGe}$ , and  $\text{UCoGe}$ , for which a recent review and comparison has been provided by Aoki, Ishida, and Floquet.[7]

Several features of  $\text{UTe}_2$  have been revealed. The susceptibility is highly anisotropic, being much higher (as temperature is lowered) along the  $\hat{a}$  axis. This anisotropy indicates that ferromagnetic ordering is more highly favored along this axis, though ordering does not actually occur in zero magnetic field. This anisotropy implies in turn a strong crystal field anisotropy of the U atom, from which any magnetic moment must arise.  $\text{UTe}_2$  remains metallic with a large (enhanced) Sommerfeld coefficient  $\gamma \approx 120 \text{ mJ/K}^2$ , [5, 6] indicative of a Kondo lattice fermionic ground state. Without any electronic structure

---

\*Electronic address: pickett@physics.ucdavis.edu

study for comparison, the degree of enhancement remains an open question. Aoki *et al.*[6] have reported a 10% entropy imbalance at  $T_c$  between the observed state and the extrapolated normal state, which may indicate some more complex behavior below  $T_c$ .

While U metallic  $5f$  electrons become highly conducting at low T, the magnetic susceptibility at higher temperature (above 150K) is characteristic of a local Curie-Weiss moment, reported variously as somewhat anisotropic with values in the  $3.3\text{-}3.6\mu_B/U$  range,[4] or also as  $2.8\mu_B/U$ . [5] This local-itinerant dichotomy is itself not so unusual, as elemental Fe itself and several heavy fermion materials behave similarly. What is different about U is that spin-orbit coupling is very large, so pure spin differentiation gives way to spin-orbit coupled quantum designations with the orbital contribution being larger than that of the spin.

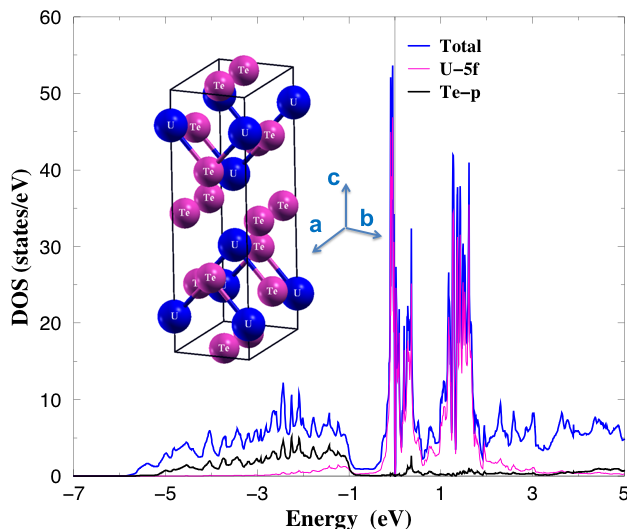


FIG. 1: Total and projected densities of states/eV (per unit cell) for nonmagnetic  $UTe_2$  from the LSDA+U(OP) functional, with projections for U  $5f$  (red) and Te  $p$  (black). The  $Immm$   $UTe_2$  crystal structure is shown in the inset: blue spheres are U, pink spheres are Te.

The structure of  $UTe_2$  is characterized by a shortest U-U distance of  $3.78\text{\AA}$  along a “chain” in the  $a$  direction, with the next distance being  $4.16\text{\AA}$ . This separation is well above Hill limit, implying that the  $5f$  electrons should be localized and magnetic. The two U sites in the cell are related by inversion. As mentioned, strong magnetic anisotropy in  $\chi_{\alpha\alpha}(T)$  establishes  $\hat{a}$  as the easy axis, but this raises the question why no magnetic order down was detected down to 2K.

Calculations indicate that FM order is strongly favored over antiferromagnetic ordering, when spins are aligned along the  $\hat{a}$  direction. The MCA is very large, nearly 100 meV, indicating that indeed FM alignment along  $\hat{a}$  is favored, and order must be being avoided by fluctuations. The large MCA indicates that crystal fields on the U site should be scrutinized.

We find, as expected, that U  $5f$  states dominate the region around the Fermi level, described in Sec. III. Inclusion of correlation effects appropriate for a more localized description versus a fully itinerant description, by including a repulsive Hubbard  $U$  interaction and a Hund’s  $J$  parameter, do not change the primary features but do lead to an effective degeneracy that may be relevant. The states at and below  $E_F$  are dominated by  $j = \frac{5}{2}$  character (spin opposite to the orbital moment). Within this multiplet,  $m_j = -\frac{5}{2}$  and  $-\frac{3}{2}$  states are fully occupied. The  $m_j = \pm\frac{1}{2}$  states provide the primary component of Fermi level states, and they are effectively degenerate and half-filled. These projections are with respect to the  $\hat{a}$  axis, chosen as the majority spin direction. Furthermore, decomposition into spin states reveals that states around  $E_F$  are essentially fully spin-polarized. These characteristics are suggestive of an incipient broken symmetry that might account for the Bogoliubov Fermi surface, and in Sec. IV some analysis is provided. A brief summary is provided in Sec. V.

## II. METHODS

The electronic structure has been investigated with the LSDA+U method, reviewed and analyzed in Ref. [8]. Fully anisotropic repulsive orbital interactions  $U_{m,m'}$  are included between all U orbitals  $m$ , with Hund’s coupling  $J_{m,m'}$  between parallel spin electrons, both treated in a fully rotationally invariant manner.[9] In the case of strong spin-orbit coupling (SOC) appropriate for U, to treat the strong orbital character realistically the spherical average interaction

$$\Delta E_{SS}^{ee} = \frac{1}{2}(\bar{U} - \bar{J})\left(\text{Tr}[\hat{n}] - \text{Tr}[\hat{n}\hat{n}]\right) \quad (1)$$

is considered as discussed in Ref. [10]. Here  $\hat{n}$  is the orbital occupation matrix of the open shell and  $\bar{U}, \bar{J}$  are spherically averaged interactions. The remaining spin and orbitally dependent LSDA+U terms include the SOC induced anisotropic contributions to the on-site Coulomb interactions – the orbital polarization (OP) – and the spin-flip terms due to spin off-diagonal matrix elements of the on-site occupation matrix  $\hat{n}_{j_z, j'_z}$ .

We use the relativistic version of the full-potential linearized augmented plane wave (FP-LAPW) method including SOC, with the rotationally invariant form of DFT+U implemented as described in Ref. [9, 11]. An additional non-spherical double-counting correction is used, described in Refs. [11, 12]. Following a conventional approach, we make use of reduced atomic Hartree-Fock values [13] of the Slater integrals  $F_2 = 6.20$  eV,  $F_4 = 4.03$  eV, and  $F_6 = 2.94$  eV. The resulting values are Hund’s  $J = 0.51$  eV, and we select a Hubbard  $U (=F_0)$  equal to the value of  $J$ . With the choice of the Coulomb repulsion  $U$  equal to the Hund’s exchange  $J$ , all spherically symmetric terms in the rotationally invariant  $U, J$  correction are set to zero, as they are treated in the LSDA

functional. This approach can be regarded as the orbital polarization (OP) limit of LSDA+U; orbital polarization functionals with DFT/[14, 15] might also be tried. For complete clarity, the functional we use is presented in detail in Appendix A.

### III. ANALYSIS OF RESULTS

#### A. Non-magnetic LDA+U(OP)

As a reference point we first perform non-magnetic LSDA+U(OP) calculations. The electronic density of states (DOS), together with the U atom  $f$ -projected DOS and Te  $p$ -projected DOS, are shown in Fig. 1. The  $\frac{5}{2}$  and  $\frac{7}{2}$  peak centers are separated by  $\sim 1$  eV. The  $\xi\vec{s}\cdot\vec{\ell}$  term in the Kohn-Sham equation has a coefficient  $\xi_{5f}=220$  meV, giving a  $\frac{5}{2} - \frac{7}{2}$  splitting of 0.77 eV, confirming that this separation is from SOC, with minor crystal field contributions. The calculated  $5f$  occupation within the U sphere  $n_f=2.8$ , which supports the viewpoint of an underlying  $f^3$  configuration. Additional evidence for this will appear later. A filled Te  $p$  shell, *i.e.*  $\text{Te}^{2-}$ , would require  $\text{U}^{4+} f^2$ , so the Te  $p$  shell is not filled and, in spite of the small U  $5f$  bandwidth, U-Te hybridization cannot be discounted.

The narrow  $5f$  electron states shown in Fig. 1 that straddle the Fermi energy ( $E_F$ ) in Fig. 1 have  $j = \frac{5}{2}$  character; the  $j = \frac{7}{2}$  manifold is centered 1.5 eV above  $E_F$ . Careful determination of the bands and DOS reveals a gap of 13 meV, apparently an “accidental” hybridization gap rather than one between characteristic bands (bonding-antibonding, specific  $m_j$  characters, etc.) Due to a flatness of the  $f$  bands there is a strong peak in the DOS (up to 35 states/eV) just 15 meV below  $E_F$  which would correspond to  $\gamma=41$  mJ K $^{-2}$  mol $^{-1}$ . Even that value is much smaller than the experimental value of  $\gamma=120$  mJ K $^{-2}$  mol $^{-1}$  [5], indicating a substantial dynamical enhancement which, considering the Kondo-like behavior observed in the resistivity, is likely due to magnetic fluctuations.

An enlargement of the band structure near  $E_F$  is shown in Fig. 2. Simple non-magnetic, uncorrelated  $\text{UTe}_2$  is calculated to be a semimetal, similar to that found by Aoki *et al.* [6] using LDA without correlation corrections. The 13 meV bandgap just above  $E_F$  reflects a hybridization gap occurring between a heavy and a light band, although the band structure is more involved than the textbook viewpoint. The semimetallic character of nonmagnetic  $\text{UTe}_2$  might suggest an instability toward electron-hole pairing [16] though there is no evidence of such a new phase. Also, we find in the next section that OP changes the Fermi level electronic structure substantially.

The  $|m_l, m_s\rangle$  and  $|m_j = m_l + m_s\rangle$  decompositions of  $N(E_F)$  are provided in Table I of Appendix B. Since the experimental susceptibility is highly anisotropic at low T, being much higher along the  $\hat{a}$  axis, we chose it as the moment quantization axis and it will be used below

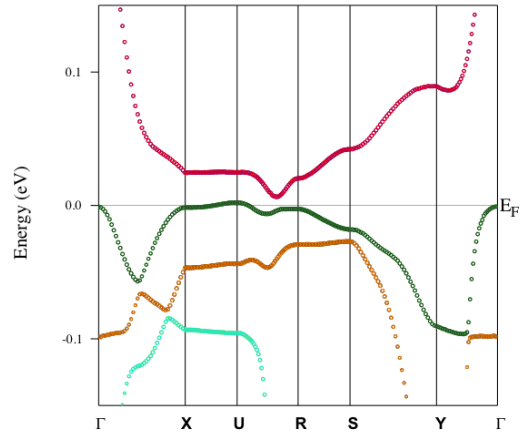


FIG. 2: The band structure and the FS from non-magnetic LSDA+U(OP) calculations. The circle size indicates the amount of  $f$ -character of the eigenstates.

in the results for ferromagnetic alignment. The major contribution to the FS comes from  $m_l = 0, m_s = -\frac{1}{2}$  and  $m_l = -1, m_s = +\frac{1}{2}$  in equal amounts, providing the orbital and spin composition of the active orbitals. Given the strong SOC of U, the angular momentum coupled representation is more fundamental. The decompositions  $|j = \frac{5}{2}, m_j = \pm\frac{1}{2}\rangle$  states (henceforward, this notation will be  $|\frac{5}{2}, \pm\frac{1}{2}\rangle$ ) plus some non-negligible amount of  $|\frac{5}{2}, \pm\frac{5}{2}\rangle$  states are dominant.

In Appendix C information on the composition of the bands near  $E_F$  is provided. The “fat-band” structure is shown in Fig. 6 emphasizing the  $|m_l, m_s\rangle$  and  $|m_j = m_l + m_s\rangle$  character of the  $j = \frac{5}{2}$  manifold, for negative  $m_j$ .

#### B. Ferromagnetic LSDA+U(OP)

No magnetic order has been detected down to 0.4K. However, based on the observed susceptibility and strong magnetocrystalline anisotropy (MCA) from both theory and experiment, slow long-range FM correlations with alignment along the  $\hat{a}$ -axis are expected, *i.e.* locally the electronic structure is FM. To model this low T phase we have performed FM calculations with spin moments (and in this collinear calculation, the orbital moments as well) aligned along the  $\hat{a}$  axis. The FM state is 185 meV/f.u. lower in the energy than the non-magnetic state. The  $f$ -shell ordered moments, oriented along the  $\hat{a}$ -axis, are calculated to be

$$\vec{M} \parallel \hat{a}: M_S=1.92\mu_B, M_L=-3.44\mu_B, M_J=-1.52\mu_B,$$

$$\vec{M} \parallel \hat{b}: M_S=1.83\mu_B, M_L=-3.71\mu_B, M_J=-1.88\mu_B,$$

$$\vec{M} \parallel \hat{c}: M_S=1.91\mu_B, M_L=-3.97\mu_B, M_J=-2.06\mu_B.$$

An analogous calculation for FM  $\text{UGe}_2$  gave  $M_S=1.32\mu_B, M_L=-2.92\mu_B, M_J=-1.58\mu_B$ , which was in good agreement with experimental data [17] in

the ordered state.

The Curie-Weiss moment, an average over fluctuations in all dimensions, is  $2.8\mu_B$  [5] to  $3.3\mu_B$  [6] for  $UTe_2$ . It is common, when moments are not strongly localized, that the ordered moment is reduced due to mixing with the conduction states. Lack of ordering in  $UTe_2$  precludes comparison, but substantial itinerant character of the moment is apparent. Calculating the magnetocrystalline anisotropy, we find that for moments oriented along the  $\hat{b}$  and  $\hat{c}$  axes, the energy is higher by 37 meV/f.u. and 96 meV/f.u. respectively. Thus, there is a strong uniaxial magnetic anisotropy, with  $\hat{a}$  being the easy axis.

The effect of allowing FM moment development and alignment is displayed in Fig. 3. The strong spin- and orbital-polarization coupled with strong SOC results in washing out of the small hybridization gap calculated for the nonmagnetic system. The value of  $N(E_F)$  is 16 states/eV-cell corresponding to a band value of  $\gamma_o=19$  mJ/K<sup>2</sup>, leaving a factor of five enhancement due to dynamic processes to account for the observed Sommerfeld coefficient.

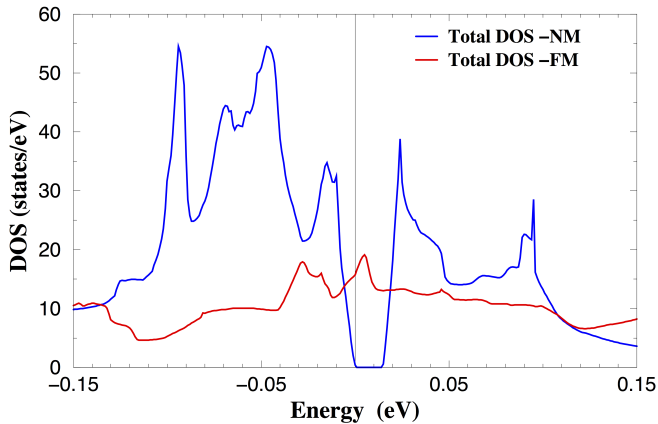


FIG. 3: Comparison of the density of states for ferromagnetic alignment (metallic) with that of the gapped nonmagnetic state, on a fine energy scale. The 13 meV gap is thoroughly washed out when magnetic moments are allowed to emerge and align.

The density of states for FM ordered  $UTe_2$ , projected onto spin directions, is displayed in Fig. 4A. The exchange splitting is seen to be around 1.5 eV, with negligible population of minority spin  $5f$  orbitals – the  $f$  shell of U is fully spin-polarized, however SOC mixes the spin moment amongst the  $m_j$  states. The U  $j_z$ -projected DOS for both  $j = \frac{5}{2}$  and  $j = \frac{7}{2}$  subspaces is pictured in Fig. 4B. The fully occupied states arise from  $j = \frac{5}{2}$  states with  $j_z = -\frac{5}{2}$  and  $-\frac{3}{2}$ . The  $j_z = \pm\frac{1}{2}$  states are half-filled, a point we return to below; higher  $j_z$  states are unfilled. The U atom configuration can thus be characterized as an  $f^2$  local moment, with  $j_z = \pm\frac{1}{2}$  orbitals that are itinerant and whose spins compensate.

The Fermi surface for FM order is displayed in Fig. 5. It has 4 sheets, with the most obvious characteristic be-

ing a strong nesting feature for FS-3 near  $(0, \frac{\pi}{b}, 0)$ . Such nearly parallel sheets, one-dimensional in character, suggest instabilities toward order that would double the cell along the  $\hat{b}$  axis. The  $|m_j = m_l + m_s\rangle$  decompositions of  $N(E_F)$  are given in Table II of Appendix B. The corresponding  $|m_l, m_s\rangle$  decompositions of  $N(E_F)$  are provided in Appendix B in Table III. From Table II, it can be observed that FS-2 has strong  $j_z = \frac{1}{2}$  character while FS-4 has strong  $j_z = -\frac{1}{2}$  character, with some  $j_z = \pm\frac{1}{2}$  character spread over the other sheets.

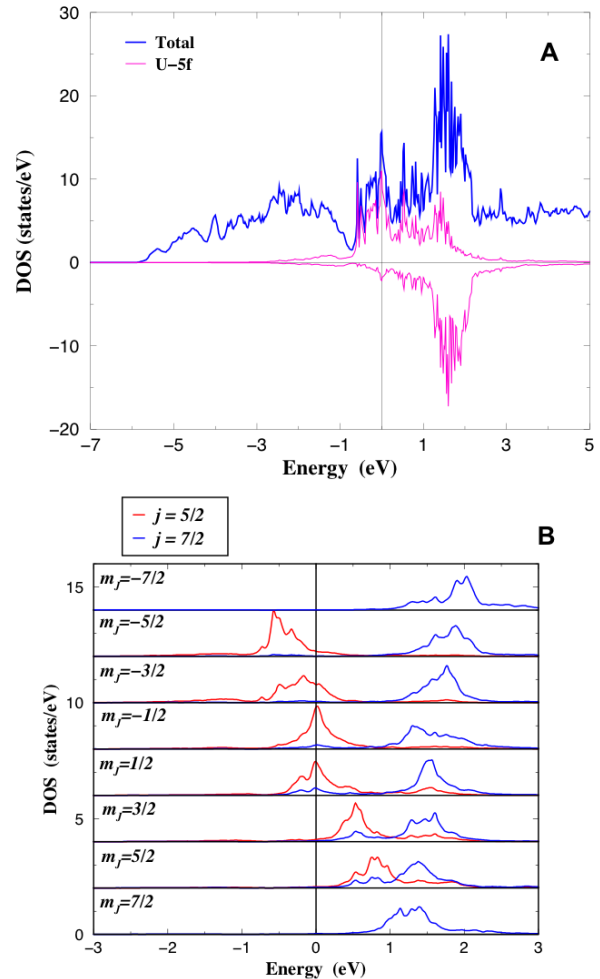


FIG. 4: Total (A) and  $f$ -projected (B) densities of states for ferromagnetic  $UTe_2$  from LSDA+U(OP) functional, with the moment along  $\hat{a}$ . (A) The  $j_z$ -decomposed DOS for both  $j = \frac{5}{2}$ , plotted upward in red, and  $j = \frac{7}{2}$ , plotted downward. (B) The  $j_z$  projected density of states, with projections stated in the panels. Occupied states arise almost entirely from  $j = \frac{5}{2}$  states with negative  $j_z$ .

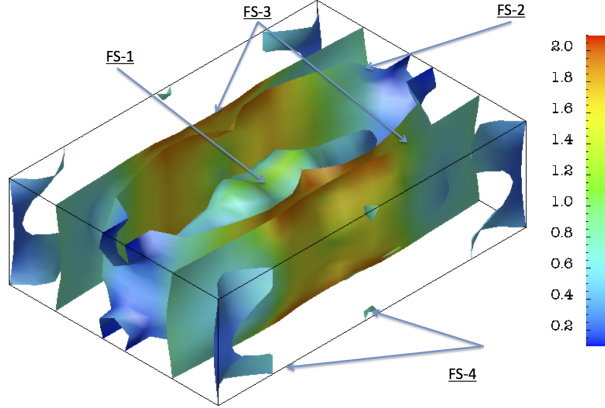


FIG. 5: Fermi surface for FM order, from LSDA+U(OP), centered at the  $\Gamma$  point. The Fermi surface is large and multi-sheeted, with a nesting feature for FS-3 near  $(0, \frac{\pi}{b}, 0)$ . FS-1 is in the center; FS-2 parallels FS-3 along parts of its length. The low velocities, given by the colorbar, extend over at least an order of magnitude, up to nearly  $2 \text{ eV}\cdot\text{\AA}$  ( $\sim 2.5 \times 10^7 \text{ cm/s}$ ).

#### IV. CONSIDERATIONS FOR PARTIAL PAIRING

Heat capacity data[5, 6] indicates that half of the fermionic carriers remain ungapped below  $T_c$ , the other half gapped by superconductivity. A central issue is that no information is yet available on the “halves” that might be involved. With a multisheeted FS with complex shape, it is difficult to identify half of the Fermi surface for gapping, barring the trivial and unphysical dividing of the zone into halves, quarters, or eights according to the  $Immm$  symmetry. The spin-up – spin-down possibility viewpoint, for example, does not have an obvious proclivity to gap exactly half of a complex Fermi surface when SOC is strong, while pairing only one spin would suggest time-reversal symmetry breaking.

We have suggested that at low T near  $T_c$ , the long-range and slow magnetic fluctuations imply that  $\text{UTe}_2$  is locally FM. In this case spin degeneracy is broken, and moreover strong SOC mixes the two spins with orbital characters. The bands and Fermi surfaces are non-degenerate, but inversion provides  $\varepsilon_{-k} = \varepsilon_k$  as the only degeneracy. Averaging over the moment fluctuations restores moment symmetry on a time scale slower than that of the fluctuation time. The next consideration is that the resistivity indicates that Kondo coherence has restored a translationally invariant state (“screened the moments”) that does not scatter carriers. This coherence and lack of broken symmetry suggests that degeneracy, viz. up-down, is restored. On the other hand, the large susceptibility implies that strong moment fluctuations remain present.

#### A. Local spin-orbital considerations.

The degeneracy of the  $m_j = \pm \frac{1}{2}$  orbitals and their half filling suggests considering linear combinations of the degenerate orbitals, which are themselves linear combinations of  $5f$  orbitals and spin projections. The spin-orbit coupled combinations of  $m_j = \pm \frac{1}{2}$  states are[18]

$$\begin{aligned}\phi_{\frac{5}{2},+\frac{1}{2}} &= -\sqrt{\frac{3}{7}}Y_{3,0}|\uparrow\rangle + \sqrt{\frac{4}{7}}Y_{3,+1}|\downarrow\rangle \\ \phi_{\frac{5}{2},-\frac{1}{2}} &= -\sqrt{\frac{3}{7}}Y_{3,-1}|\uparrow\rangle + \sqrt{\frac{4}{7}}Y_{3,0}|\downarrow\rangle\end{aligned}\quad (2)$$

in terms of spherical harmonics  $Y_{\ell,m}$  and spin projections. Each state contains  $Y_{3,0}$  but with opposite spin projections. Rotating these degenerate orbitals in functional space so the common orbital  $Y_{3,0}$  has equal spin-up and -down amplitudes leads to

$$\begin{aligned}\Phi_{\pm} &= [\sqrt{\frac{4}{7}}\phi_{\frac{5}{2},+\frac{1}{2}} \pm \beta\sqrt{\frac{3}{7}}\phi_{\frac{5}{2},-\frac{1}{2}}], \\ &= [\sqrt{\frac{16}{49}}Y_{3,+1}|\downarrow\rangle \mp \beta\sqrt{\frac{9}{49}}Y_{3,-1}|\uparrow\rangle] \\ &\quad + \sqrt{\frac{24}{49}}Y_{3,0}\frac{[-|\uparrow\rangle \pm \beta|\downarrow\rangle]}{\sqrt{2}}\end{aligned}\quad (3)$$

where  $\beta = 1$  or  $\beta = i$ . This linear combination leads to the orbital function  $Y_{3,0}$  with vanishing orbital moment and a specific spin projection:  $\langle \vec{s} \rangle = (0, \pm 1, 0)$ , which has zero projection along the orbital  $z$ -axis, which due to the large magnetic anisotropy is the crystalline  $\hat{a}$ -axis. The other part has entwined ( $Y_{3,\pm 1}$ ) orbitals with opposite spin projections. A second intriguing observation is that one part has a fraction  $\frac{25}{49} = 51\%$  of the weight, while the second contains 49%; these fractions are experimentally indistinguishable from the “one half” of carriers that became paired at  $T_c$  in  $\text{UTe}_2$ . These observations suggest possible symmetry breaking that links the magnetic anisotropy with the orbital occupation, a possible line for further consideration.

#### B. The coherent-carrier itinerant picture

The Fermi liquid behavior, evidenced by the strong decrease in the resistivity by a factor of up to 35 below 50K,[6] reflects Kondo screening of the  $5f$  moments. While the large susceptibility, arising from field alignment of magnetic fluctuations, indicates dynamic moments, they no longer scatter carriers, primarily just contributing a mass enhancement which we can estimate is of the order of a factor of five.

Aoki, Ishida, and Floquet have observed in their review[7] that only uranium compounds have been confirmed as FM superconductors: orthorhombic  $\text{UXGe}$ ,  $X=\text{Ge, Rh, Co}$ . The latter two are isovalent. We obtain an  $f^3$  configuration in  $\text{UTe}_2$ , just as has been con-

cluded experimentally for UCoGe,[7] so the  $f^3$  configuration may carry importance.

For weak ferromagnets and incipient ferromagnets, DFT methods are known to overestimate the tendency toward magnetic order and the size of magnetic moments, usually ascribed to neglect of magnetic fluctuation effects in the functionals, and possibly to the necessity to include dynamic effects explicitly. Our work provides the groundwork for modeling the metallic Fermi liquid phase of UTe<sub>2</sub> that provides the platform for an exotic superconducting state. In UPt<sub>3</sub> for example, the six-sheeted Fermi surface is given very realistically by LDA methods.[19–23] In several cases, however, Fermi surfaces are not predicted well by first principles methods.

Our work provides important guidelines: the heavy fermion Fermi liquid state of UTe<sub>2</sub> is built on an  $f^3$  U configuration in which  $m_j = \pm\frac{1}{2}$  states in the  $j = \frac{5}{2}$  subspace provides the primary orbital content of the Fermi surface states  $|k, n, \tau\rangle$ . Here  $\tau$  indicates the pseudospin component that bears some characteristics of the more common spin degree of freedom that is commonly used to categorize exotic pairing states. The specific spin-orbital decompositions discussed in the previous subsection may deserve further consideration.

## V. DISCUSSION AND SUMMARY

UTe<sub>2</sub> presents the usual challenges of a Kondo lattice superconductor, with the complicating features of strong magnetic anisotropy (strong SOC) and (especially) the coexistence of normal carriers and superconducting pairs below  $T_c$ . At low T magnetic fluctuations slow down, especially those with large moments as observed in UTe<sub>2</sub>. Considering the strong evidence, both experimental and theoretical, of an easy  $\hat{a}$  axis and strong magnetocrystalline anisotropy, a outstanding question is how UTe<sub>2</sub> manages to avoid magnetic order. Kondo screening of the moments is the primary rationalization.

Comparison and contrast of UTe<sub>2</sub> and UPd<sub>2</sub>Al<sub>3</sub> [25] are striking. Both have comparable specific heat  $\gamma$ 's indicating Kondo lattice character arising from spin fluctuations, and both become superconducting at 1.7-1.8K. Both can be characterized as a local moment from a localized  $f^2$  pair or orbitals, with roughly one more  $5f$  electron being itinerant. However, UPd<sub>2</sub>Al<sub>3</sub> orders antiferromagnetically at six times higher than  $T_c$ , compared to UTe<sub>2</sub> which (according to muon spin rotation data[26]) does not order magnetically down to 25 mK. And of course, only half the carriers in UTe<sub>2</sub> become superconducting. Evidently the phases in these intermetallic uranium compounds are sensitive to several relative energy scales.

We have explored the possibility that at low T (somewhat above the superconducting  $T_c$ ) there is medium range FM orientation of the U moments, from  $j = \frac{5}{2}$  states (quantization axis is the  $\hat{a}$  axis) which have strong localized character (moments around  $2-3\mu_B$ ) but strong

enough hopping to enable conducting behavior with correlation enhancements. In this case the U sites are locally ferromagnetic, involving essentially pure spin (majority) moments. Magnetic (exchange) coupling proceeds through the spin moments, so the single spin character of the calculated moments become relevant. In the limit of negligible SOC and one spin channel being frozen out, triplet pairing reduces to single-spin superconducting pairing[27, 28] suggested as a possibility in half-metals.

As mentioned in the Introduction, Agterberg and collaborators have pointed out the possibility of symmetry restricted ‘‘Bogoliubov Fermi surfaces:’’ areas of Fermi surfaces that remain ungapped in the superconducting state and give, among other effects, a non-zero Sommerfeld coefficient above the superconducting ground state. With no obvious symmetry(s) beyond the space group in the calculated Fermi surface and global time-reversal symmetry, there is no apparent reason why the normal fraction should be (within uncertainty) half of the number of carriers in the normal state. Can this ‘‘50%’’ fraction be accidental? It hardly seems likely.

We have presented a scenario for this division: the Clebsch-Gordon coupling enforced by strong SOC suggests a coupling that favors the choice of spatially uniform, orbital-moment free, spin-mixed spin orbitals as the building blocks for the Bloch orbitals that will eventually pair. The linear combination that suggests the importance of these orbitals contains 49% of the Fermi level spectral density of  $j_z = \pm\frac{1}{2}$  states that are calculated to be effectively degenerate in the correlated band structure of this heavy fermion compound. The half-filled nature of these  $j_z = \pm\frac{1}{2}$  orbitals, with density of states peaking at  $E_F$ , suggests the tendency toward symmetry-breaking states.

The simplest scenario for the apparent Bogoliubov Fermi surface carriers observed in superconducting UTe<sub>2</sub> is the simple separation (spin-up versus -down) used by Ran et al., adapted to this compound. In terms of pairing of the  $j_z = \pm\frac{1}{2}$  orbitals, triplet pairing involves the space of  $J = 0, \pm 1$  pairs

$$\Delta(k) = d_0\Delta_0(k) + d_1\Delta_1(k) + d_{-1}\Delta_{-1}(k) \quad (4)$$

in the usual notation.[29] Strong on-site ferromagnetic alignment raises the first terms with its antialigned moments to high energy. Then the vanishing of (say)  $\Delta_{-1}$  results in a superconducting phase with  $J = 1$  pairs gapped and the remaining 50% of carriers residing on a Bogoliubov Fermi surface. The microscopic source of such symmetry breaking, if it occurs, remains for further studies.

## VI. ACKNOWLEDGMENTS

W.E.P. thanks P. Hirschfeld for an introduction to the Bogoliubov Fermi surface literature and concepts, and comments on the manuscript. A.B.S. acknowledges

partial support from MSMT Project No. SOLID21-CZ.02.1.01/0.0/0.0/16\_019/0000760, and GACR grant No. 18-02344S. W.E.P. was supported by NSF Grant DMR 1607139.

### Appendix A: The exchange-correlation functional

The electron-electron interaction energy  $E^{ee}$  in the DFT+U total-energy functional, with the spin-orbit coupling (SOC) included [24], has the form

$$E^{ee} = \frac{1}{2} \sum_{\gamma_1 \gamma_2 \gamma_3 \gamma_4} n_{\gamma_1 \gamma_2} \left( V_{\gamma_1 \gamma_3; \gamma_2 \gamma_4}^{ee} - V_{\gamma_1 \gamma_3; \gamma_4 \gamma_2}^{ee} \right) n_{\gamma_3 \gamma_4} \quad (\text{A1})$$

which contains the 14x14 on-site occupation matrix  $n_{\gamma_1 \gamma_2} \equiv n_{m_1 \sigma_1, m_2 \sigma_2}$  with generally non-zero orbital and spin off-diagonal matrix elements. The  $V^{ee}$  is an effective on-site Coulomb interaction, expressed in terms of Slater integrals (see Eq.(3) in Ref. [9]) which are linked to intra-atomic repulsion  $U_{m, m'}$  and exchange  $J_{m, m'}$  quantities mentioned in Sec. II. The spherically symmetric double-counting energy  $E^{dc}$  is subtracted from  $E^{ee}$  to correct on the electron-electron interaction already included in DFT.

The DFT+U energy correction  $\Delta E^{ee} = E^{ee} - E^{dc}$  can be divided into a sum of spherically symmetric and anisotropic terms. In the case of the "atomic" or "fully localized" (FLL) limit of  $E^{dc}$ , and without SOC, the spherically-symmetric part is given by [10],

$$\Delta E^{ee} = \frac{(U - J)}{2} \left( \text{Tr}[\hat{n}] - \text{Tr}[\hat{n}\hat{n}] \right) \quad (\text{A2})$$

The choice  $U = J$  in Eq. (A1) means that the spherically symmetric part of  $\Delta E^{ee}$  given by Eq. (A2) becomes equal to zero. The remaining non-spherically symmetric part of  $\Delta E^{ee}$  can be regarded as the DFT+U analog of the proposed "orbital polarization correction" functionals (OPC).[14, 15]

Due to the full potential character, care should be taken to exclude the so-called "non-spherical double counting" of the  $f$ -state nonspherical contributions to the DFT and DFT+U parts of the Kohn-Sham potential. When the atomic sphere matrix elements of the DFT+U Hamiltonian are calculated, those contributions from the lattice harmonics  $K_\nu$  of the nonspherical part of the DFT potential  $V_{DFT}^{NSH}(\mathbf{r}) = \sum_\nu V_\nu(r) K_\nu(\hat{r})$  are removed, which are proportional to  $\langle l m_1 | K_\nu | l m_2 \rangle$  for  $l = 3$ , the  $f$ -states orbital quantum number.

### Appendix B: Decomposition of the U 5f DOS at $E_F$

This table provides the stated decomposition of the Fermi level density of states.

TABLE I: The  $|m_l, m_s\rangle$  and  $|j, m_j\rangle$  decompositions of the U atom  $f$ -projected DOS at  $E_F$  (in states/eV unit cell) for the unpolarized system. The magnetic quantization is along the easy  $\hat{a}$  axis.

$m_l$	-3	-2	-1	0	1	2	3	
spin- $\uparrow$	0.16	0.04	0.10	0.16	0.01	0.03	0.00	
spin- $\downarrow$	0.00	0.03	0.01	0.16	0.10	0.04	0.16	
$m_j$	-7/2	-5/2	-3/2	-1/2	1/2	3/2	5/2	7/2
	0	0.19	0.05	0.26	0.26	0.05	0.19	0

TABLE II: Decomposition of the four Fermi surface contributions to  $N(E_F)$  from  $|m_j = m_l + m_s\rangle$  projections, for FM aligned UTe<sub>2</sub>. Magnetic quantization is along the  $\hat{a}$  axis. The dominance of the  $j_z = \pm \frac{1}{2}$  is evident.

$m_j$	-7/2	-5/2	-3/2	-1/2	1/2	3/2	5/2	7/2
FS1	0	0.02	0.17	0.15	0.25	0.01	0.03	0.01
FS2	0	0.08	0.21	0.71	1.35	0.06	0.03	0.01
FS3	0	0.05	0.23	0.63	0.36	0.04	0.02	0.01
FS4	0	0.04	0.27	1.30	0.48	0.04	0.02	0.01
Sum	0	0.19	0.88	2.79	2.44	0.15	0.10	0.04

### Appendix C: 5f orbital contribution near $E_F$

This array of figures provides the relative amounts of the stated spin-orbital characters of states near the Fermi level. The bands on the zone boundary X-U-R-S are flatter. More dispersion occurs along  $\Gamma$ -X and S-Y.

TABLE III: The  $|m_l, m_s\rangle$  decomposition of  $N_f(E_F)$  (eV<sup>-1</sup>), for ferromagnetic alignment of UTe<sub>2</sub> along the  $\hat{a}$  axis. The down spin components are small; as noted in the text, the system is near full spin polarization..

FS1							
$m_l$	-3	-2	-1	0	1	2	3
spin- $\uparrow$	0.02	0.14	0.10	0.20	0.01	0.02	0.01
spin- $\downarrow$	0.00	0.00	0.03	0.05	0.05	0.00	0.01
FS2							
spin- $\uparrow$	0.08	0.18	0.60	1.12	0.04	0.02	0.01
spin- $\downarrow$	0.00	0.00	0.03	0.11	0.23	0.02	0.01
FS3							
spin- $\uparrow$	0.05	0.20	0.52	0.30	0.02	0.02	0.01
spin- $\downarrow$	0.00	0.00	0.03	0.11	0.06	0.02	0.01
FS4							
spin- $\uparrow$	0.04	0.24	1.07	0.40	0.01	0.01	0.01
spin- $\downarrow$	0.00	0.00	0.03	0.23	0.08	0.01	0.01

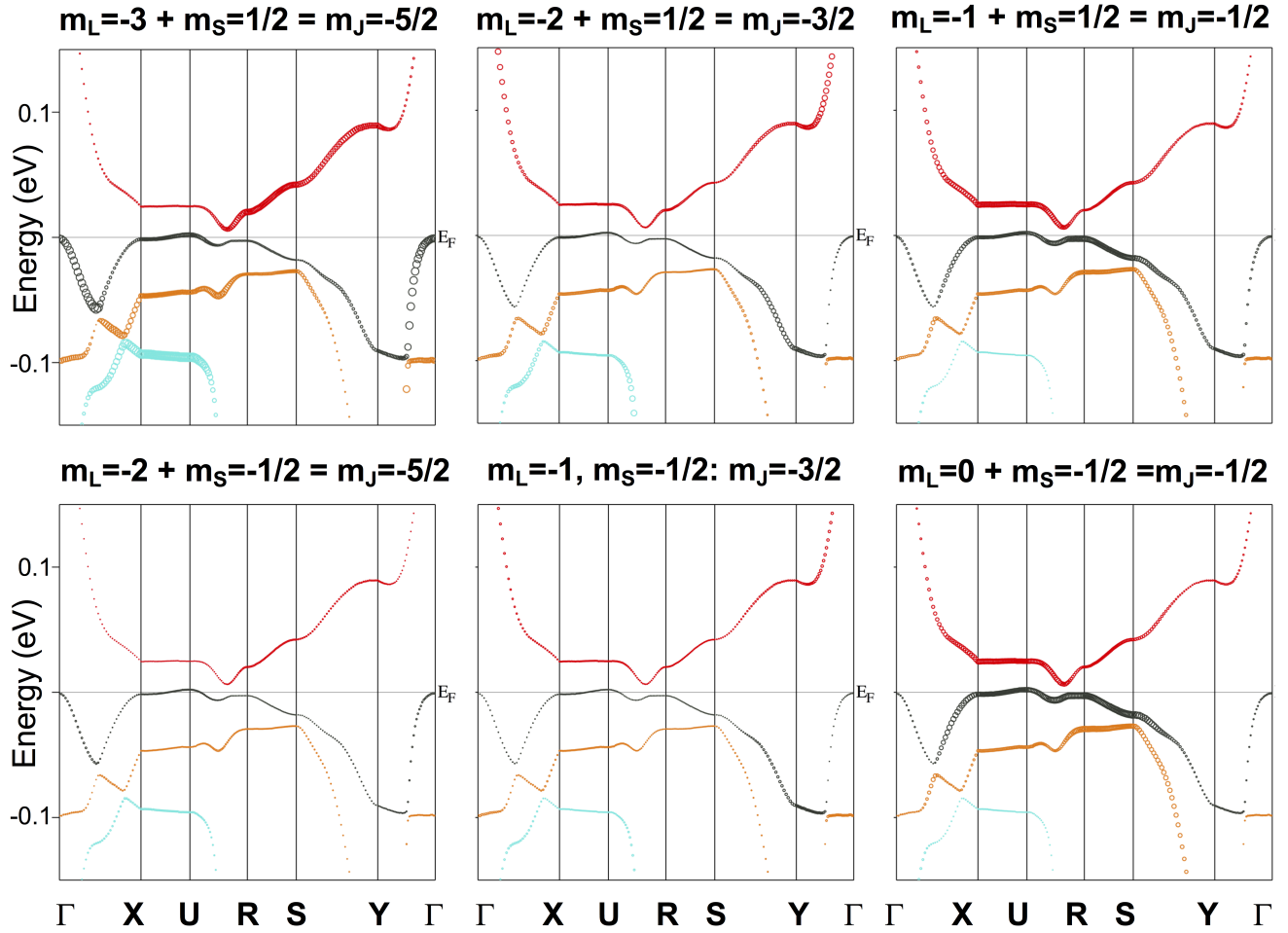


FIG. 6: The 5f fat-band structure of non-magnetic UTe<sub>2</sub> from LDA+U(OP) calculation. The circle size indicates the amount of  $j = \frac{5}{2}, m_j$  character in the bands, as indicated. The two contributions to the  $j_z = -\frac{5}{2}$  character are quite different; the differences in the other two cases is not so pronounced. Note that the full energy range is only 300 meV.



- [1] D. F. Agterberg, P. M. R. Brydon, and C. Timm, Bogoliubov Fermi Surfaces in Superconductors with Broken Time-reversal Symmetry, *Phys. Rev. Lett.* **118**, 127001 (2017).
- [2] Y. Sato, S. Kasahara, T. Taniguchi, X. Xing, Y. Kasahara, Y. Tokiwa, Y. Yamakawa, H. Kontani, T. Shibauchi, and Y. Matsuda, Abrupt change of the superconducting gap structure at the nematic critical point in  $\text{FeSe}_{1-x}\text{S}_x$ , *PNAS* **115**, 1227 (2018).
- [3] C. Setty, S. Bhattacharyya, A. Kreisel, and P. Hirschfeld, Ultranodal pair states in iron-based superconductors, arXiv:1903.00481.
- [4] S. Ikeda, H. Sakai, D. Aoki, Y. Homma, E. Yamamoto, A. Nakamura, Y. Shiokawa, Y. Haga, and Y. Onuki, Single Crystal Growth and Magnetic Properties of  $\text{UTe}_2$ , *J. Phys. Soc. Japan* **75** (Suppl.), 116 (2006).
- [5] S. Ran, C. Eckberg, Q.-P. Ding, Y. Furukawa, T. Metz, S. R. Saha, I.-L. Liu, M. Zic, J. Paglione, and N. P. Butch, Spontaneously polarized half-gapped superconductivity, arXiv:1811.11808.
- [6] D. Aoki, A. Nakamura, F. Honda, D. Li, Y. Homma, Y. Shimizu, Y. J. Sato, G. Knebel, J.-P. Brison, A. Pourret, D. Braithwaite, G. Lapertot, Q. Niu, M. Valiska, H. Harima, and J. Flouquet, Unconventional Superconductivity in Heavy Fermion  $\text{UTe}_2$ , *J. Phys. Soc. Japan* **88**, 043702 (2019); arXiv:1903.02410.
- [7] D. Aoki, k. Ishida, and J. Floquet, Review of U-based Ferromagnetic Superconductors: Comparison between  $\text{UGe}_2$ ,  $\text{URhGe}$ , and  $\text{UCoGe}$ , *J. Phys. Soc. Japan* **88**, 043702 (2019).
- [8] E. R. Ylvisaker, K. Koepf, and W. E. Pickett, Anisotropy and Magnetism in the LSDA+U Method, *Phys. Rev. B* **79**, 035103 (2009).
- [9] A. B. Shick, A. I. Liechtenstein, and W. E. Pickett, Implementation of the LDA+U method using the full-potential linearized augmented plane-wave basis, *Phys. Rev. B* **60**, 10763 (1999).
- [10] S. L. Dudarev, G. A. Botton, S. Y. Savrasov, C. J. Humphreys, and A. P. Sutton, Electron-energy-loss spectra and the structural stability of nickel oxide: An LSDA+U study *Phys. Rev. B* **57**, 1505 (1998).
- [11] A. B. Shick, V. Janis, V. Drchal, W. E. Pickett, Spin and orbital magnetic state of  $\text{UGe}_2$  under pressure, *Phys. Rev. B* **70**, 134506 (2004).
- [12] O. Kristanovski, A. B. Shick, F. Lechermann, and A. I. Liechtenstein, Role of nonspherical double counting in DFT+DMFT: total energy and structural optimization of pnictide superconductors, *Phys. Rev. B* **97**, 201116(R) (2018).
- [13] K. T. Moore and G. van der Laan, Nature of the 5f states in actinide metals, *Rev. Mod. Phys.* **81**, 235 (2009).
- [14] O. Eriksson, M. S. S. Brooks, and B. Johansson, Orbital polarization in narrow-band systems: Application to volume collapses in light lanthanides, *Phys. Rev. B* **41**, 7311 (1990).
- [15] H. Eschrig, M. Sargolzaei, K. Koepf, and M. Richter, Orbital polarization in the Kohn-Sham-Dirac theory, *EPL* **72**, 611 (2005).
- [16] B. A. Volkov, Yu. V. Kopaev, and A. I. Rusinov, Theory of “excitonic” ferromagnetism, *Zh. Eksp. Teor. Fiz.* **68**, 1899 (1975).
- [17] N. Kernavanois, B. Grenier, A. Huxley, E. Ressouche, J.-P. Sanchez, and J. Flouquet, Neutron scattering study of the ferromagnetic superconductor  $\text{UGe}_2$ , *Phys. Rev. B* **64**, 174509 (2001).
- [18] L. D. Landau and I. M. Lifshitz, *Quantum Mechanics: Non-relativistic Theory* (Pergamon, Oxford, 1958), p. 408.
- [19] C. S. Wang, H. Krakauer, and W. E. Pickett, Electronic structure and mass enhancement of the heavy fermion superconductor  $\text{UPt}_3$ , *Physica B&C* **135**, 34 (1985).
- [20] C. S. Wang, H. Krakauer and W. E. Pickett, Unconventional superconductivity and normal-state properties in the heavy fermion superconductor  $\text{UPt}_3$ , *J. Phys. F* **16**, L287 (1986).
- [21] M. R. Norman, R. C. Albers, A. M. Boring, and N. E. Christensen, Fermi surface and effective masses for the heavy-electron superconductor  $\text{UPt}_3$ , *Solid State Commun.* **68**, 245 (1988).
- [22] C. S. Wang, M. R. Norman, R. C. Albers, A. M. Boring, W. E. Pickett, H. Krakauer, and N. E. Christensen, Fermi surface of  $\text{UPt}_3$  within the local-density approximation, *Phys. Rev. B* **35**, 7260 (1987).
- [23] G. J. McMullan, P. M. C. Rourke, M. R. Norman, A. D. Huxley, N. Doiron-Leyraud, J. Flouquet, G. G. Lonzarich, A. McCollam and S. R. Julian, *New J. Phys.* **10**, 053029 (2008).  
Electronic structure and hyperfine interactions for light actinide impurities in bcc Fe: Spin-polarized relativistic calculations, *Phys. Rev. B* **49**, 12860 (1994).
- [24] I. V. Solovyev, A. I. Liechtenstein, and K. Terakura, Is Hund’s Second Rule Responsible for the Orbital Magnetism in Solids? *Phys. Rev. Lett.* **80**, 5758 (1998).
- [25] Y. Tokunaga *et al.*,  $^{125}\text{Te}$ -NMR Study on a Single Crystal of Heavy Fermion Superconductor  $\text{UTe}_2$ , *J. Phys. Soc. Japan* (in press), arXiv:1906.01303.
- [26] S. Sudar *et al.*, Coexistence of ferromagnetic fluctuations and superconductivity in the actinide superconductor  $\text{UTe}_2$ , arXiv:1905.06901.
- [27] W. E. Pickett, Single Spin Superconductivity, *Phys. Rev. Lett.* **77**, 3185 (1996).
- [28] R. E. Rudd and W. E. Pickett, Single Spin Superconductivity: Formulation and Ginzburg-Landau Theory, *Phys. Rev. B* **57**, 557 (1998).
- [29] V. P. Mineev, Superconductivity in uranium ferromagnets, *Physics - Uspekhi* **60**, 121 (2017).